

# Structural Decompositions for End-to-End Relighting

Thomas Nestmeyer\*

MPI for Intelligent Systems, Tübingen, Germany

tnestmeyer@tue.mpg.de

Jean-François Lalonde\*

Université Laval, Quebec City, Canada

jflalonde@gel.ulaval.ca

Iain Matthews\*

Epic Games, Pittsburgh, USA

iain.matthews@epicgames.com

Andreas M. Lehrmann

Facebook Inc., Pittsburgh, USA

andreas.lehrmann@gmail.com

## Abstract

*Relighting is an essential step in artificially transferring an object from one image into another environment. For example, a believable teleconference in Augmented Reality requires a portrait recorded in the source environment to be displayed and relit consistent with the light configuration of the destination scene.*

*In this paper, we investigate architectures for learning to both de-light and relight an image of a human face end-to-end. The architectures vary in how much they enforce physically-based image formation and rendering constraints. The most structured model decomposes the input image into intrinsic components according to a diffuse physics-based image formation model and augments the render to relight including non-diffuse effects. An intermediate model uses fewer intrinsic constraints and the least structured model makes no assumptions on the image formation.*

*To train our models and evaluate the approach, we collected portraits of 21 subjects with various expressions and poses, each in a sequence of 32 individual light sources in a controlled light stage setup. Our method leads to precise and believable relighting results in challenging illumination conditions and poses, including when the subject is facing away from the camera. We compare our method to state-of-the-art relighting approaches and illustrate its superiority in a series of quantitative and qualitative experiments.*

## 1. Introduction

In recent years, augmented reality (AR) has seen widespread adoption across a variety of fields, including gaming, communication, and remote work. For an AR experience to be immersive and believable, it is crucial that

the virtual objects inserted in the environment match the lighting conditions of their (real) surroundings even if they were originally captured in an environment with different lighting. This task, known as *relighting*, has a long history in computer vision and comprises a pool of seminal works paving the way for modern AR technologies [2,3,22,33,37].

Any approach attempting to solve this relighting problem is faced with two critical architectural design choices: the definition of internal representations and the definition of processes operating on these internal representations. Depending on the shape and meaning of these two elements, we can place each model somewhere along an axis describing the extent of its *structural assumptions*.

On one end of this axis, image-to-image translation approaches relying on deep learning architectures (e.g. [17]) make no structural assumption about the relighting problem. Provided with enough representational capacity, such an end-to-end system can describe any underlying process but is prone to large variance due to over-parametrization, poor generalization due to physically implausible encodings, and difficult test-time manipulation due to semantically meaningless internal states. While this could potentially be alleviated with more training data, acquiring sufficient amounts is very time consuming.

On the other end of the axis, relighting has long been represented as a physics-based, two-stage process. First, *de-light* the object in order to recover its intrinsic properties of reflectance, geometry, and lighting. Second, *relight* the object according to a desired target lighting. This implies an exact instantiation of the rendering equation [4] operating on lighting and surface reflectance representations capable of capturing the true nature of the light-material-geometry interactions. In practice, this is infeasible and imperfect parametric assumptions are unavoidable. Typical approximations include smooth lighting (e.g. with low-order spherical harmonics) and diffuse materials [2,37], which do not correspond to real-world objects. An important example

\*This work was performed while the authors were at the Facebook Reality Labs Pittsburgh, USA.

are human faces, which are known for their challenging interactions with light, including view-dependent specularities, subsurface scattering, hard cast shadows, and spatially-varying reflectance.

Recent approaches have demonstrated that explicitly integrating physical processes in neural architectures is beneficial in terms of both, robust estimates from limited data and increased generalization due to the optimization process’ coerced focus on a formation process rather than a data representation [27, 37, 41]. However, these approaches have focused on the *de-lighting* process, and use the simplified physical models for relighting, thereby not modeling non-diffuse effects such as cast shadows and specularities.

In this work, we bridge the gap between the expressiveness of a physically implausible end-to-end approach and the robustness of a structurally imperfect physics-based approach. In particular, we consider relighting as an image-to-image translation problem and propose a structured generator dividing the relighting task into two distinct components: a physics-based parametric rendering of estimated intrinsic components and a physics-guided residual refinement to address violations of structural assumptions. Specifically, our image formation model makes the assumption of directional light and diffuse materials. The subsequent refinement process is *conditioned* on the components inferred during this step (i.e., albedo, normals, and diffuse rendering) and can thus dynamically account for shadows and any remaining non-diffuse phenomena.

Our work builds upon previous solutions to physics-based relighting and makes the following four novel contributions. First, we propose two neural architectures that combine the strengths of a physics-guided relighting process with the expressive representations of a deep neural network. Of critical difference with previous work which focuses on de-lighting only, our approach simultaneously learns to both *de-light and relight*. Second, we describe how this hybrid approach allows modeling of realistic, non-diffuse material effects and show results on a novel dataset of human faces under varying lighting conditions and poses. Third, we perform a comprehensive ablation study along an architectural axis with progressively higher amount of physical structure and validate our contributions with respect to various popular evaluation metrics. Finally, we compare our architecture to state-of-the-art relighting approaches and illustrate its superiority in a series of quantitative and qualitative experiments.

## 2. Related Work

**Intrinsic images.** Factoring images into their intrinsic components of reflectance, shape and illumination has long been studied in computer vision. Intrinsic image decomposition [3] and the related problem of shape from shading [52] have, for the past decades, inspired countless de-

rived works. Of interest, Barron and Malik [2] propose to simultaneously recover shape, illumination, reflectance and shading from a single image, and rely on extensive priors to guide an inverse rendering optimization procedure. Other methods recover richer lighting representations in the form of environment maps given the known object shape [28]. More recent approaches rely on deep learning architectures for the same task, for example using a combination of CNN and guided/bilateral filtering [30] or a pure end-to-end CNN approach [11]. These data-driven methods have to deal with the common problem that ground truth data is hard to come by. Available datasets consist of sparse relative reflectance judgments [5] or sparse shading annotations [21], which limits learning and quantitative evaluation. Therefore, researchers have also relied on synthetic data (combined with these datasets) for this task [26, 36].

**Relighting.** While many previous works focus on lighting estimation either from objects [2, 13, 28] or even entire images [12, 16, 19, 49, 50], few papers explicitly focus on the *relighting* problem. Of note, Ren et al. [34] use a small number of images as input, and, more recently, [48] learn to determine which set of 5 light directions is optimal for relighting. When relighting from a single image as we do in this work, Cabral et al. [8] propose a method that is specialized for tree canopies.

**Faces.** Lighting estimation from face images has long focused on normalization for improving face recognition. For example, [46] use spherical harmonics (SH) to relight a face image, and [44] uses a Markov random field to handle sharp shadows which cannot be handled by low-frequency SH models. Other face modeling methods have exploited rough lighting estimates (often in SH) in order to reconstruct the geometry [24, 42] or texture [25]. In the computer graphics literature, similar ideas have been proposed for face replacement [6, 10].

Low-frequency lighting estimation from a face image has been explored in [20, 38, 39]. In contrast, Nishino and Nayar [31] note that eyes reflect our surroundings and can be used to recover high frequency lighting, provided that sufficient image resolution is available. More closely related to our work, Calian et al. [9] learn the space of outdoor lighting using a deep autoencoder, and combine this latent space with an inverse optimization framework to estimate outdoor lighting from a face. However, their work is restricted to outdoor lighting, and cannot be used explicitly for relighting.

Of particular relevance to our work, neural face editing [41] and the related SfSNet [37] train neural networks to decompose a face image into surface normals, albedo, and spherical harmonics lighting. These approaches impose a loss on each of the intrinsic components, as well as a

rendering loss which ensures that the *combination* of these components is similar to the input image. In contrast, the portrait lighting transfer approach of [40] bypasses the need for decomposition, and instead transfers the illumination from a reference portrait to an input photograph to create high-quality relit images. Recently, FRADA [23] revisited the idea of relighting for improving face recognition, and used face-specific 3D morphable models (similar to [41]). In our work, we do not impose any face-specific template, and explore the different types of decompositions that can be learned by a network, and how they apply to the challenging case of relighting with strong directional lighting.

### 3. Architecture

The following two sections first introduce an image formation process (Sec. 3.1) and then describe its integration into a physics-based relighting architecture (Sec. 3.2).

#### 3.1. Image Formation Process

An image formation process describes the physics-based operations transforming the image-projected scene intrinsics on a 3D surface to a rendered output. While any such process can only be an approximation to reality, the majority of physics-based works are based on specific instantiations of the rendering equation [18],

$$L_o(\omega_o) = \int_{\omega_i \in \Omega} f(\omega_i, \omega_o) \langle \mathbf{n}, L_i(\omega_i) \cdot \omega_i \rangle d\omega_i, \quad (1)$$

where  $\omega_i, \omega_o$  are the incoming and outgoing light directions relative to the surface normal  $\mathbf{n}$  at the surface point  $\mathbf{X}_j$ . Furthermore,  $L_i(\omega_i)$  and  $L_o(\omega_o)$  are the corresponding (ir)radiances,  $f(\cdot, \cdot)$  is the BRDF describing the material’s reflectance properties, and  $\langle \mathbf{n}, \omega_i \rangle$  is the weakening factor due to Lambert’s cosine law.

**Diffuse Lighting.** Despite this model’s limitations, e.g., its lack of subsurface scattering, it is routinely simplified even further by assuming a diffuse decomposition into albedo  $a \in \mathbb{R}$  and shading  $s \in \mathbb{R}$ ,

$$a = f(\omega_i, \omega_o), \quad [\text{const.}] \quad (2)$$

$$s = \int_{\omega_i \in \Omega} \langle \mathbf{n}, L_i(\omega_i) \cdot \omega_i \rangle d\omega_i. \quad (3)$$

Note that, while  $a$  is constant for fixed  $\mathbf{X}_j$ , different image pixels  $\mathbf{x}_j$  look at different 3D surface points  $\mathbf{X}_j$ , leading to spatially varying albedo and shading maps.

**Non-diffuse Effects.** A realistic relighting approach must relax the restrictive modeling assumptions of Eq. (1) (no subsurface scattering, transmission, polarization, etc.)

and Eq. (2) (no specularities). Unfortunately, learning a spatially varying BRDF model  $f(\omega_i, \omega_o)$  based on an expressive, non-parametric representation is infeasible: assuming an image size of  $256 \times 256$  and a pixelwise discretization of the local half-angle space similar to [29] would result in a total of  $5.7 \cdot 10^{11}$  parameters. Learning a low-dimensional representation in terms of semantic parameters [7] seems like a viable alternative but is still prone to overfitting and would, even if successful, not account for light-material-interactions outside of its parametric space.

Consequently, we propose to take a hybrid approach and decompose  $f(\omega_i, \omega_o)$  into two principled components: a diffuse component  $a$  and a light-varying residual  $r(\omega_i, \omega_o)$ , turning Eq. (1) into

$$f(\omega_i, \omega_o) = a + r(\omega_i, \omega_o), \quad (4)$$

$$L_o(\omega_o) = as + \int_{\omega_i \in \Omega} r(\omega_i, \omega_o) \cdot \langle \mathbf{n}, L_i(\omega_i) \cdot \omega_i \rangle d\omega_i.$$

Under the assumption of a single directional light source with intensity  $I(\tilde{\omega}_i)$  in the direction of  $\tilde{\omega}_i$  and writing  $\tilde{r}(\tilde{\omega}_i, \omega_o) = r(\tilde{\omega}_i, \omega_o) \cdot \langle \mathbf{n}, I(\tilde{\omega}_i) \cdot \tilde{\omega}_i \rangle$ , we have

$$L_o(\omega_o) = (as + \tilde{r}(\tilde{\omega}_i, \omega_o)) \cdot v(\tilde{\omega}_i), \quad (5)$$

where we have identified  $L_i(\tilde{\omega}_i) = I(\tilde{\omega}_i) \cdot v(\tilde{\omega}_i)$  and  $v(\tilde{\omega}_i) \in \{0, 1\}$  is the binary visibility of the light source from  $\mathbf{X}_j$ . Eq. (5) will serve as the underlying image formation process in all subsequent sections. While  $as$  captures the bulk of the diffuse energy across the image according to an explicit generative model, the residual  $\tilde{r}(\tilde{\omega}_i, \omega_o)$  accounts for physical effects outside of the space representable by Eq. (2) and will take the form of a neural network. We do not impose any assumptions on  $r(\omega_i, \omega_o)$ , allowing light subtraction, but expect  $a$  to be close to the albedo of an actual diffuse model, such as the ones typically used in photometric stereo [47], which we use to infer guidance signals from our captured data (see Sec. 4.1).

**Discussion.** While directional lights are conceptually simple, they lead to very challenging relighting problems. Our combination of an explicit diffuse rendering process and a non-diffuse residual (with implicit shading) serves several purposes: (1) Describing most of the image intensities with a physics-based model means the output image will be more consistent with the laws of physics; (2) Describing specular highlights with small residuals instead of a full image takes heavy burden from the CNN; (3) Leaving the residual unconstrained (up to ground truth guidance) allows us to model effects that are not explainable by the BRDF, such as subsurface scattering; (4) Modeling visibility explicitly helps, because the often imposed simple diffuse model does not handle cast shadows. At the same time, expecting the residual to take care of shadow removal by resynthesis is much harder than just masking it.

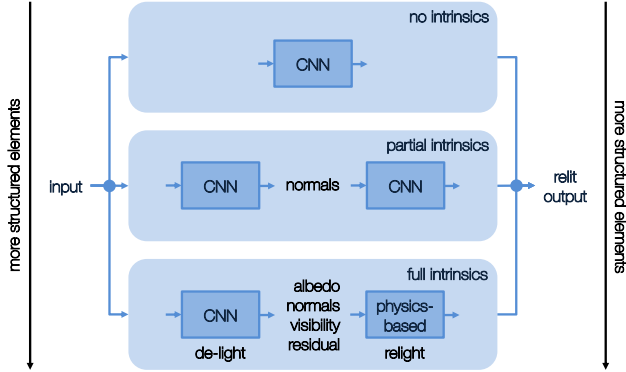


Figure 1: **Structured Generators.** We use a conditional GAN [17] and approach relighting as a supervised image-to-image translation problem with a structured generator. We propose and explore a series of progressively more structured generators to leverage physics: no explicit prediction of intrinsic factors (top), prediction of normals but processing of those normals with a CNN (middle), and prediction of all intrinsic factors required to compute an explicit physics-based rendering (bottom).

### 3.2. Physics-Guided Relighting

Presented with an input image  $I_{src}$  that was lit by an input illumination  $l_{src}$ , our goal is to learn to relight  $I_{src}$  according to a desired output illumination  $l_{dst}$ ,

$$G(I_{src}, l_{src}, l_{dst}) = I_{dst}. \quad (6)$$

At training time, we assume  $l_{src}$  and  $l_{dst}$  to be directional lights, which is known to be a particularly challenging instance of relighting and accurately matches our actual data (see Sec. 4). At test time, this is not a limitation, since we can easily fit a set of directional lights to an environment map to perform more complex relighting (see Sec. 5.3).

We view Eq. (6) as a supervised image-to-image translation problem and use conditional GANs [17] as our underlying framework. This leaves us with the choice of a suitable generator  $G$ . We consider three options differing in the extent of their structured elements (see Fig. 1):

**No Intrinsic.** The arguably simplest way to learn Eq. (6) from data is to instantiate  $G$  as a traditional CNN consisting of a series of generic layers with no semantic meaning and no knowledge of the image formation process, such as the popular U-Net architecture [35].

**Partial Intrinsic.** Given that the input  $I_{src}$  and relit output  $I_{dst}$  share a common BRDF, the majority of the information required for relighting is contained in the geometry of the object. One way to leverage this insight is to enforce a physics-inspired intermediate prediction in the form

of normals and supply the corresponding shading image (inferred from the desired output lighting) to the subsequent layers of the CNN. We achieve this with a dedicated loss on an internal normals layer comparing the local prediction to a guidance signal obtained from a photometric stereo method [47]. While this is not enough information to generate the relit output based on an explicit rendering process, it should provide critical information to the remaining layers of the CNN to be superior to the previously discussed variant with no intrinsic guidance.

**Full Intrinsic.** The most principled inverse-graphics approach to solving the relighting task consists of a recognition model inferring intrinsic components from observed images (de-lighting) and a generative model producing relit images from intrinsic components (relighting). While the recognition model takes the form of a traditional CNN, the generative model follows our image formation process (Sec. 3.1) and is represented by a series of structured layers with clear physical meaning. In line with Eq. (5), we implement the latter as a two-stage process: (Stage 1) Using the desired target lighting, we compute shading from predicted normals and multiply the result with our albedo estimate to obtain a diffuse render; (Stage 2) Conditioned on all intrinsic states predicted in stage 1, we infer a residual image and a visibility map, which we combine with the diffuse render according to Eq. (5). An illustration of these two stages is shown in Fig. 2.

We introduce losses for all internal predictions, i.e., albedo, normals, shading, diffuse rendering, visibility, and residual. We emphasize the importance of using the right loss function and refer to Sec. 5.1 for a comprehensive study regarding this choice. In order to obtain the corresponding guidance, we use an off-the-shelf photometric stereo solution [47]. All operations along this pipeline are differentiable, which allows us to learn the proposed model in an end-to-end fashion.

## 4. Data

Our data comprises a diverse set of facial expressions captured under various lighting conditions. The following sections give a detailed overview of the acquisition (Sec. 4.1) and augmentation (Sec. 4.2) process.

### 4.1. Acquisition

We record our data in a calibrated multi-view light-stage consisting of 6 stationary Sony PMW-F55 camcorders and a total of 32 white LED lights. The cameras record linear HDR images at  $1080 \times 2048 / 60$  fps and are synchronized with a Blackmagic Sync Generator that also triggers the LED lights. We flash one LED per frame and instruct our subjects to hold a static expression for the full duration



Figure 2: **Physics-Guided Relighting with Structured Generators.** Our generator consists of two stages modeling diffuse and non-diffuse effects. All intrinsic predictions are guided by losses w.r.t. photometric stereo reconstructions. **(a)** We use a U-Net with grouped convolutions to make independent predictions of the intrinsic components. Given a desired output lighting, we compute shading from normals and render a diffuse output. **(b)** Conditioned on all modalities inferred in **(a)**, we predict a non-diffuse residual and binary visibility map to model specularities, cast shadows, and other effects not captured by our instance of the rendering equation.

of an LED cycle (32 frames  $\sim 0.53s$ ). In order to minimize movements, we let the subjects trigger the recordings themselves while leaning their heads against a head rest. Furthermore, we filter our data based on the difference of two fully lit shots before/after each cycle. For light calibration, we use a chrome sphere to recover directions and intensities in 3D [14], but subsequently express the 6 cameras with respect to their image planes, such that we obtain a total of  $6 \cdot 32 = 192$  different light directions/intensities during a single LED cycle.

All together, we record a total of 482 sequences from 21 subjects, resulting in a total of  $482 \cdot 6 \cdot 32 \cdot 32 = 2,961,408$  relighting pairs. Each relighting pair is formed using any one of the 32 lights as input, and any one as output, taken from the same sequence and same camera. We split them into 81% training (17 subjects), 9.5% validation (2 subjects) and 9.5% testing (2 subjects) sets.<sup>1</sup> We did not ask the subjects to follow any specific protocol of facial expressions besides being diverse, such that our evaluation on validation/test data is on *both* unseen expressions and unseen subjects.

After extraction of the raw data, we use an off-the-shelf photometric stereo reconstruction (PMS) method [47] to separate the input images  $I$  into albedo  $A$ , shading  $S$  and non-diffuse residual images  $R = I - A \odot S$  per frame.

## 4.2. Augmentation

Modern neural architectures are much better at interpolation than extrapolation. It is therefore critical to cover the space of valid light transports as well as possible. To this end, we perform a series of data augmentations steps in an attempt to establish strong correlations throughout

<sup>1</sup>The split into training, validation and test set was done manually in an effort to balance the demographics of the small amount of subjects. See Appendix A.1 for details.

the parametric relighting space: (1) We flip all training images along the horizontal and vertical axis, increasing the effective dataset size by a factor of 4. Note that this also requires adaption of the corresponding light directions and normals; (2) We perform a linear scaling  $x' = s \cdot x$ ,  $s \sim \mathcal{U}_{[0.6, 1.1]}$ , of the images, shading, residuals and light intensities. In practice, we did not observe substantial benefits compared to training without light augmentation; (3) We randomly perturb the light calibration with Gaussian noise  $n \sim \mathcal{N}(0, 0.01^2)$  to improve generalization and account for minimal calibration errors; (4) For quantitative results, we perform a spatial rescaling to  $\frac{1}{8}$ th of the original image resolution ( $135 \times 256$ ), to train on *random crops* of size  $128 \times 128$  and test on center crops with the same resolution to have comparability with SfSNet. Qualitative results are generated by rescaling to  $\frac{1}{2}$  of the original resolution ( $540 \times 1024$ ), to train on *random crops* of size  $512 \times 768$  and test on center crops of that resolution.

## 5. Experiments

Our models were implemented using the PyTorch framework [32] with the U-Net [35] generator and GAN [15] discriminator based on the implementations provided by pix2pix [17]. The images in our dataset are converted from camera RAW and represented as 16-bit linear RGB values nominally in the range  $[0, 1]$ . There is under- and over-shoot headroom, but for training and evaluation we clamp them into this range and linearly transform to  $[-1, 1]$  as input into the network. Predicted normals are always renormalized to unit vectors. During training, losses are backpropagated from foreground (i.e. lit) pixels only.

## 5.1. Evaluation metric

Quantitatively comparing the relit prediction  $\hat{I}_{\text{dst}}$  of the generator against the ground truth  $I_{\text{dst}}$  requires an appropriate error measure. We consider the  $L_1$  and  $L_2$  norm, but recognize they do not coincide with the human perceptual response. We also consider the *perceptual* loss suggested by [51] using the distance of features of a CNN pretrained on *Imagenet*. Another prevailing metric of image quality assessment is structural similarity (SSIM) and its multi scale variant (MS-SSIM) [45]. We actually take the dissimilarity measure,

$$\text{DSSIM} = \frac{1 - \text{SSIM}}{2} \quad (7)$$

and likewise for MS-SSIM, to adhere to the concept of consistently reporting errors.

When defining the loss function during training the same choices of distance metrics are available. To densely evaluate their performance, we report in Table 1 the results of training all intrinsic layers with the same loss function from the options above.

We note that, for our task, using SSIM for the training loss consistently leads to models which generalize better on the validation set using all of the error metrics. The only exception is evaluation using the perceptual metric, which is better when also trained using this metric. Therefore we chose the models trained on SSIM for computing the final test results.

## 5.2. Baseline Comparison

We compare all of our proposed architectures qualitatively (Fig. 3), as well as quantitatively (Table 2) to related work. In particular, we compare methods in the scenario where the input lighting direction is both known and unknown.

### 5.2.1 Baselines

**PMS.** To understand the possible lower limit of a diffuse model, we take albedo  $A$  and shading  $S$  from photometric stereo (PMS) and diffuse render via  $A \odot S$ . We note that this model has access to all light configurations at the same time, with the desired target illumination amongst them, so has an unfair advantage. For this reason we do not highlight results for this model in Table 2.

**SfSNet.** We take the pretrained state-of-the-art network of [37] and apply it to our data by using their decomposition into albedo and normals, but ignoring the output spherical harmonics estimate. We compute target shading as the dot product of  $\ell_{\text{dst}}$  and normals to have a direct comparison with our assumption of directional light and present the result after diffuse rendering.

Table 1: **Loss Selection.** We explore the influence of different training losses and evaluation metrics on 3 models with different degrees of structured guidance. For each class, we show validation scores for all pairwise combinations of 5 training losses (rows) and the same 5 evaluation metrics (columns). The best model for each evaluation metric is shown in bold. SSIM/MS-SSIM are expressed as dissimilarities (Eq. (7)).

G	Training Loss	Evaluation Metric				
		$L_1$	$L_2$	Percept.	SSIM	MS-SSIM
none	$L_1$	.0452	.0067	.2564	.1707	.1144
	$L_2$	.0516	.0082	.2663	.1911	.1369
	Percept.	.0424	.0062	<b>.1868</b>	.1440	.0992
	SSIM	<b>.0406</b>	<b>.0055</b>	.2138	<b>.1378</b>	.0930
	MS-SSIM	.0422	.0058	.2358	.1547	<b>.0913</b>
partial	$L_1$	.0366	.0050	.2312	.1409	.0861
	$L_2$	.0410	.0056	.2641	.1628	.0968
	Percept.	.0363	.0047	<b>.1658</b>	.1282	.0785
	SSIM	<b>.0336</b>	<b>.0040</b>	.1962	<b>.1159</b>	<b>.0689</b>
	MS-SSIM	.0366	.0044	.2257	.1399	.0758
full	$L_1$	.0406	.0055	.2237	.1484	.0913
	$L_2$	.0415	.0056	.2302	.1547	.0953
	Percept.	.0365	.0048	<b>.1701</b>	.1308	.0803
	SSIM	<b>.0362</b>	<b>.0045</b>	.2008	<b>.1270</b>	<b>.0793</b>
	MS-SSIM	.0410	.0055	.2165	.1470	.0910

[G: guidance; SSIM: structured similarity; MS-SSIM: multi-scale SSIM; Percept.: perceptual loss [51]]

**SfSNet (retrained).** Our calibrated PMS data capture setup gives us access to ground truth normals and albedo image estimates that we use to retrain SfSNet [37]. Additionally, we provide the source illumination as input, to which our models also have access. Compared to the pretrained model above, this baseline can be seen as a fairer comparison to SfSNet.

**Pix2pix (no guidance).** Our instantiation of the *no guidance* baseline introduced in Sec. 3.2 is a direct extension of the pix2pix translation GAN [17]. We slightly modify their architecture by conditioning the generator on the input image as well as the source and target illumination. This ensures a fair comparison with our more structured models (partial guidance, full guidance), which may also have access to lighting information.

### 5.2.2 Evaluation

**Qualitative evaluation.** We compiled a collection of qualitative results in Fig. 3. To align the low-resolution  $128 \times 128$  pixel results obtained from SfSNet [37] with our

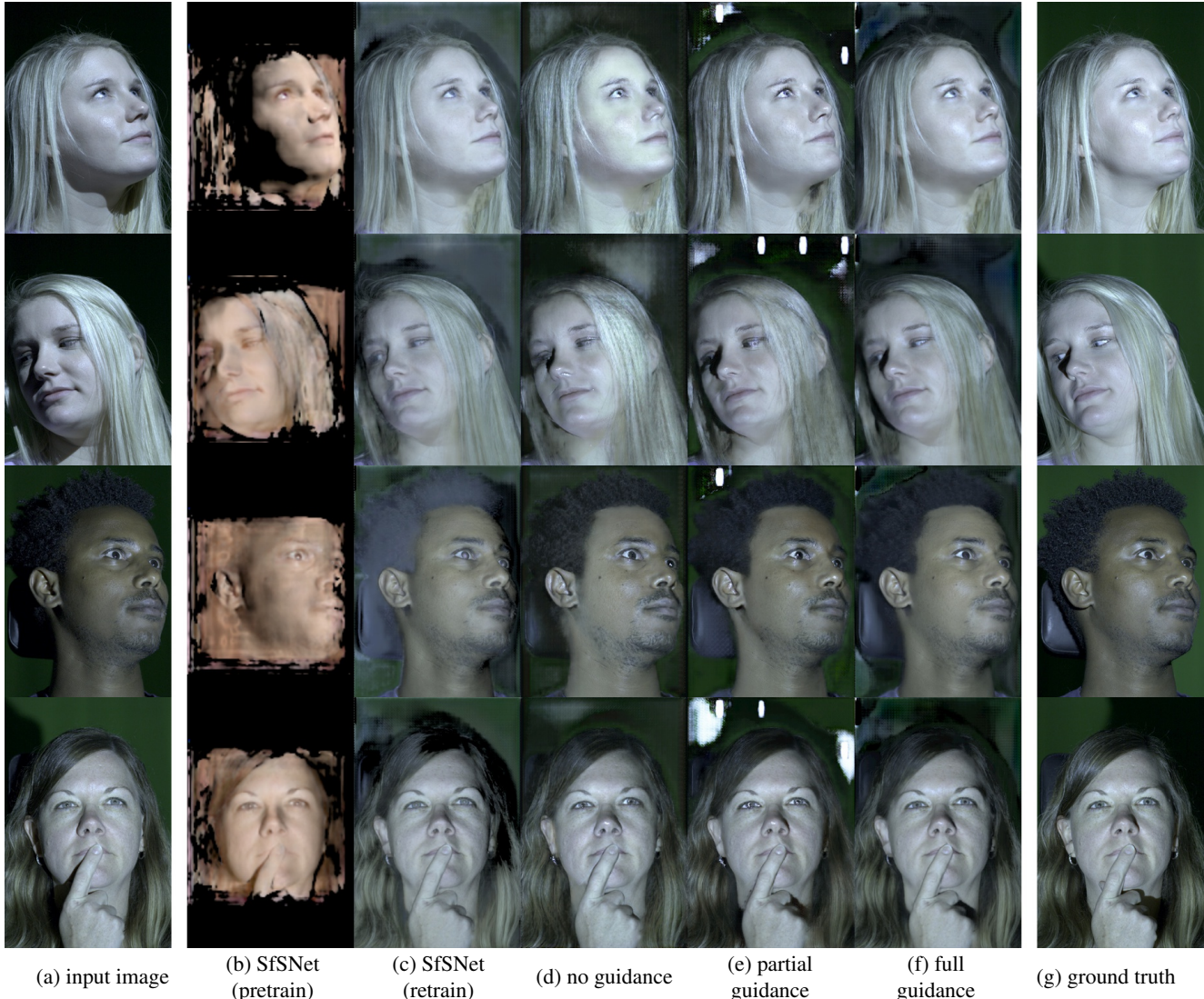


Figure 3: **Qualitative Evaluation on Unseen Subjects and Expressions.** We compare relighting (a) the input image with (b/c) pretrained and retrained variants of SfSNet [37], (d) our model with no guidance as an extension of pix2pix [17], (e) our model with partial guidance on the normals, and (f) our model with full guidance. In (g), we show the ground truth capture of the given target illumination. All results have been converted from linear to sRGB.

predictions in a resolution of  $512 \times 768$ , we scale them to a width of 512 pixels and center them vertically.

While the shading of SfSNet is smooth, it has a bias towards an albedo which probably resembles skin color in their training data and does not distinguish well between different skin tones and hair. Retraining their model on our data leads to more accurate results as expected. Still, due to the diffuse assumption, it looks flat compared to our more expressive models. It misses specularities, and surface normals orthogonal to the light direction are missing ambient light from inter-reflections.

The pretrained SfSNet model fails at more extreme head

poses. The pix2pix (no guidance) model provides promising results, but it often shows physically non-plausible artifacts. Since there is no principled relighting defined in the ‘partial guidance’ model, the prediction of the ‘full guidance’ model often leads to more believable results due to its need to estimate a consistent albedo, as can be seen for example at the hair in the second row of Fig. 3. The last row shows a hand occluding the face leading to strong cast shadows that have to be introduced/removed. Nonetheless, our models using varying intrinsic guidance all gracefully handle that case.

Although not our focus, the shadow term of the ‘full

Table 2: **Baseline Comparison.** We show a quantitative comparison of our approach to baseline methods. Performance is reported under the assumption of both known (‘with’) and unknown (‘w/o’) source illumination. All models have been trained with the SSIM loss.

L	Model/ Guidance	Evaluation Metric				
		$L_1$	$L_2$	Percept.	SSIM	MS-SSIM
	PMS	.0391	.0047	.1630	.1125	.0561
with	SfSNet (R)	.0636	.0121	.2508	.1840	.1277
	no guidance (P2P)	.0668	.0144	.2430	.1832	.1328
	partial guidance	<b>.0590</b>	<b>.0118</b>	.2195	<b>.1609</b>	<b>.1111</b>
	full guidance	.0609	.0123	<b>.2144</b>	.1618	.1138
w/o	SfSNet (P)	.1359	.0424	.4703	.3221	.3121
	no guidance (P2P)	.0815	.0189	.2783	.2076	.1623
	partial guidance	.0695	.0144	<b>.2325</b>	.1801	.1353
	full guidance	<b>.0684</b>	<b>.0142</b>	.2273	<b>.1763</b>	<b>.1316</b>

[L: access to source illumination; SSIM: structured similarity, MS-SSIM: multi-scale SSIM; Percept.: perceptual loss [51]; PMS: photometric stereo; P2P: Pix2pix [17]; P/R: (pre)trained]

guidance’ model generally learns to do matting of the background. While our data allows foreground masks computed from PMS, we wanted to show the full image predictions for better judgment. At test time, an off-the-shelf face matting approach, e.g. [43], could be used for cleaning.

In Figs. 9 and 10, we extended this comparison to related work and we encourage the reader to look at more qualitative results of this type in the supplementary video<sup>2</sup>, where we show relighting under a moving target illumination.

**Quantitative evaluation** In Table 2, we summarize the quantitative performance of our models on the test set with respect to SfSNet retrained on our data. Especially in the important columns of perceptual metrics, we outperform the diffuse baseline and show that including guidance from physics results in better performance. For reference, the PMS ground truth reconstruction, restricted to a diffuse model, is also shown.

### 5.3. Relaxations

We take a closer look at the structural assumptions underlying our model and show how to alleviate them.

**Relighting with Unknown Source Illumination.** All our models made use of the source and target illumination. While we cannot remove the need for the target illumination, information about the source illumination is already contained in the input image, allowing for implicit learning of  $\ell_{src}$ . Hence, we additionally trained each model class

<sup>2</sup><https://youtu.be/QJK6MdT79rM>



Figure 4: **Relighting with Unknown Source Illumination.** (a) Input image. (b) Relighting model *with* access to source illumination. (c) Relighting model *without* access to source illumination. (d) Ground truth output.



Figure 5: **Relighting with Environment Maps.** We relight the input (first column) w.r.t. 5 different environment maps.

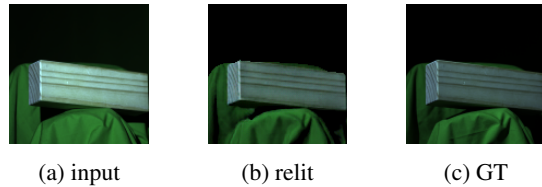


Figure 6: **Relighting of Generic Objects.** Example of a wooden block relit by our ‘full guidance’ model after training on other poses of that object. (a) Input image. (b) Relit output with masked background. (c) Ground truth output.

without access to the source illumination. As expected, we observe a small performance drop compared to the models with explicit knowledge (see Table 2 and Fig. 4). Nonetheless, our models with ‘partial’ and ‘full’ guidance, but no access to the source illumination, still achieve similar performance to the simple model without guidance, but access to the input illumination.

**Relighting with Environment Maps.** Directional light sources are a very general representation. Therefore, our approach easily allows for relighting with environment maps: we simply sample environment maps by downscaling them to  $64 \times 32$  pixels and instantiating our relighting prediction with one light direction per pixel. Since light is additive, we then mix the resulting prediction according to their color and intensity. A more principled approach, like structured importance sampling of the environment map [1], is possible but goes beyond the scope of this demonstration of relighting with arbitrary environment maps. A small ex-



ample of a relit scene with a variety of environment maps<sup>3</sup> is shown in Fig. 5 and additional results are contained in Figs. 11 and 12 and the supplementary video<sup>4</sup>.

**Relighting of Generic Objects.** Considering applications like teleconferencing in AR, our main focus so far was on relighting portraits. Due to their complex interactions with light, human faces (and skin in general) provide a great testbed for relighting. Nonetheless, our approach does not rely on any explicit face template and is thus applicable to arbitrary objects. To illustrate this fact, we train our ‘full guidance’ model on several poses of a wood block and show a relighting result of an unseen pose in Fig. 6. Note that full abstraction to arbitrary object classes would require substantially more training data and is thus left for future work.

## 6. Conclusion

We explored a series of structured relighting models ranging from a process-agnostic end-to-end system to an architecture with semantic decomposition in and subsequent re-rendering from intrinsic components. On a novel light stage dataset with challenging directional lighting, our integration of an explicit generative rendering process and a non-diffuse neural refinement layer within an end-to-end architecture proved to be superior to a model with no structural elements. A comprehensive study of different losses and evaluation metrics highlighted the benefits of training on a perceptual loss over more traditional choices. We believe our model to be useful in a wide range of face-centric and more general applications in augmented reality, such as teleconferencing, virtual try-on, and home decoration.

## References

- [1] S. Agarwal, R. Ramamoorthi, S. Belongie, and H. W. Jensen. Structured importance sampling of environment maps. In *ACM Transactions on Graphics (TOG)*, volume 22, pages 605–612. ACM, 2003. 8
- [2] J. T. Barron and J. Malik. Shape, illumination, and reflectance from shading. *IEEE transactions on pattern analysis and machine intelligence*, 37(8):1670–1687, 2015. 1, 2
- [3] H. Barrow and J. Tenenbaum. Recovering intrinsic scene characteristics. *Comput. Vis. Syst., A Hanson & E. Riseman (Eds.)*, pages 3–26, 1978. 1, 2
- [4] F. Bartell, E. Dereniak, and W. Wolfe. The theory and measurement of bidirectional reflectance distribution function (brdf) and bidirectional transmittance distribution function (btdf). In *Radiation scattering in optical systems*, volume 257, pages 154–161. International Society for Optics and Photonics, 1981. 1
- [5] S. Bell, K. Bala, and N. Snavely. Intrinsic images in the wild. *ACM Transactions on Graphics (TOG)*, 33(4):159, 2014. 2
- [6] D. Bitouk, N. Kumar, S. Dhillon, P. N. Belhumeur, and S. K. Nayar. Face swapping: automatically replacing faces in photographs. *ACM Transactions on Graphics (SIGGRAPH 2008)*, 27(3):39:1–39:8, 2008. 2
- [7] B. Burley. Physically-based shading at disney. In *SIGGRAPH 2012 Courses*, 2012. 3
- [8] M. Cabral, N. Bonneel, S. Lefebvre, and G. Drettakis. Relighting photographs of tree canopies. *IEEE transactions on visualization and computer graphics*, 17(10):1459–1474, 2011. 2
- [9] D. A. Calian, J.-F. Lalonde, P. Gotardo, T. Simon, I. Matthews, and K. Mitchell. From faces to outdoor light probes. In *Computer Graphics Forum*, volume 37, pages 51–61. Wiley Online Library, 2018. 2
- [10] K. Dale, K. Sunkavalli, M. K. Johnson, D. Vlastic, W. Matusik, and H. Pfister. Video face replacement. *ACM Transactions on Graphics (SIGGRAPH Asia 2011)*, 30(6), Dec. 2011. 2
- [11] Q. Fan, J. Yang, G. Hua, B. Chen, and D. Wipf. Revisiting deep intrinsic image decompositions. In *Proceedings of the IEEE conference on computer vision and pattern recognition*, pages 8944–8952, 2018. 2
- [12] M.-A. Gardner, K. Sunkavalli, E. Yumer, X. Shen, E. Gambaretto, C. Gagné, and J.-F. Lalonde. Learning to predict indoor illumination from a single image. *arXiv preprint arXiv:1704.00090*, 2017. 2
- [13] S. Georgoulis, K. Rematas, T. Ritschel, E. Gavves, M. Fritz, L. Van Gool, and T. Tuytelaars. Reflectance and natural illumination from single-material specular objects using deep learning. *IEEE Transactions on Pattern Analysis and Machine Intelligence*, 40(8):1932–1947, 2018. 2
- [14] D. B. Goldman, B. Curless, A. Hertzmann, and S. M. Seitz. Shape and spatially-varying brdfs from photometric stereo. *IEEE Transactions on Pattern Analysis and Machine Intelligence*, 32(6):1060–1071, 2010. 5
- [15] I. Goodfellow, J. Pouget-Abadie, M. Mirza, B. Xu, D. Warde-Farley, S. Ozair, A. Courville, and Y. Bengio. Generative adversarial nets. In *Advances in neural information processing systems*, pages 2672–2680, 2014. 5
- [16] Y. Hold-Geoffroy, K. Sunkavalli, S. Hadap, E. Gambaretto, and J.-F. Lalonde. Deep outdoor illumination estimation. In *IEEE International Conference on Computer Vision and Pattern Recognition*, 2017. 2
- [17] P. Isola, J.-Y. Zhu, T. Zhou, and A. A. Efros. Image-to-image translation with conditional adversarial networks. In *IEEE Conference on Computer Vision and Pattern Recognition (CVPR)*, 2017. 1, 4, 5, 6, 7, 8, 14, 15
- [18] J. T. Kajiya. The rendering equation. In *Proc. ACM SIGGRAPH*, pages 143–150, 1986. 3
- [19] K. Karsch, K. Sunkavalli, S. Hadap, N. Carr, H. Jin, R. Fonte, M. Sittig, and D. Forsyth. Automatic scene inference for 3d object compositing. *ACM Transactions on Graphics*, (3):32:1–32:15, 2014. 2
- [20] S. B. Knorr and D. Kurz. Real-time illumination estimation from faces for coherent rendering. In *IEEE International Symposium on Mixed and Augmented Reality*, 2014. 2

<sup>3</sup>The fire environment map (in the last column) was obtained from “BlinkFarm” ([www.youtube.com/blinkfarm](http://www.youtube.com/blinkfarm)).

<sup>4</sup><https://youtu.be/QJK6MdT79rM>

- [21] B. Kovacs, S. Bell, N. Snavely, and K. Bala. Shading annotations in the wild. In *IEEE Conference on Computer Vision and Pattern Recognition*, 2017. 2
- [22] E. H. Land and J. J. McCann. Lightness and retinex theory. *Josa*, 61(1):1–11, 1971. 1
- [23] H. Le and I. Kakadiaris. Illumination-invariant face recognition with deep relit face images. In *2019 IEEE Winter Conference on Applications of Computer Vision (WACV)*, pages 2146–2155. IEEE, 2019. 3
- [24] J. Lee, R. Machiraju, B. Moghaddam, and H. Pfister. Estimation of 3d faces and illumination from single photographs using a bilinear illumination model. In *Eurographics Conference on Rendering Techniques*, EGSR '05, pages 73–82, 2005. 2
- [25] C. Li, K. Zhou, and S. Lin. Intrinsic face image decomposition with human face priors. In *European Conference on Computer Vision*, pages 218–233, 2014. 2
- [26] Z. Li and N. Snavely. CGIntrinsics: Better intrinsic image decomposition through physically-based rendering. In *European Conference on Computer Vision*, 2018. 2
- [27] Z. Li, Z. Xu, R. Ramamoorthi, K. Sunkavalli, and M. Chandraker. Learning to reconstruct shape and spatially-varying reflectance from a single image. *ACM Transactions on Graphics (SIGGRAPH Asia)*, 37(6), Nov. 2018. 2
- [28] S. Lombardi and K. Nishino. Reflectance and illumination recovery in the wild. *IEEE transactions on pattern analysis and machine intelligence*, 38(1):129–141, 2016. 2
- [29] W. Matusik. *A data-driven reflectance model*. PhD thesis, Massachusetts Institute of Technology, 2003. 3
- [30] T. Nestmeyer and P. V. Gehler. Reflectance adaptive filtering improves intrinsic image estimation. In *Proceedings of the IEEE Conference on Computer Vision and Pattern Recognition*, pages 6789–6798, 2017. 2
- [31] K. Nishino and S. K. Nayar. Eyes for relighting. *ACM Transactions on Graphics (SIGGRAPH 2004)*, 23(3):704–711, July 2004. 2
- [32] A. Paszke, S. Gross, S. Chintala, G. Chanan, E. Yang, Z. DeVito, Z. Lin, A. Desmaison, L. Antiga, and A. Lerer. Automatic differentiation in pytorch. In *NIPS-W*, 2017. 5
- [33] P. Peers, N. Tamura, W. Matusik, and P. Debevec. Post-production facial performance relighting using reflectance transfer. In *ACM Transactions on Graphics (TOG)*, volume 26, page 52. ACM, 2007. 1
- [34] P. Ren, Y. Dong, S. Lin, X. Tong, and B. Guo. Image based relighting using neural networks. *ACM Trans. Graph.*, 34(4):111:1–111:12, July 2015. 2
- [35] O. Ronneberger, P. Fischer, and T. Brox. U-net: Convolutional networks for biomedical image segmentation. In *International Conference on Medical image computing and computer-assisted intervention*, pages 234–241. Springer, 2015. 4, 5
- [36] S. Sengupta, J. Gu, K. Kim, G. Liu, D. W. Jacobs, and J. Kautz. Neural inverse rendering of an indoor scene from a single image. *CoRR*, abs/1901.02453, 2019. 2
- [37] S. Sengupta, A. Kanazawa, C. D. Castillo, and D. W. Jacobs. Sfsnet: Learning shape, reflectance and illuminance of faces in the wild. In *Computer Vision and Pattern Recognition (CVPR)*, 2018. 1, 2, 6, 7, 14, 15
- [38] D. Shihlaei and V. Blanz. Realistic inverse lighting from a single 2d image of a face, taken under unknown and complex lighting. In *IEEE International Conference on Automatic Face and Gesture Recognition*, jul 2015. 2
- [39] H. Shim. Faces as light probes for relighting. *Optical Engineering*, 51(7):077002–1, 2012. 2
- [40] Z. Shu, S. Hadap, E. Shechtman, K. Sunkavalli, S. Paris, and D. Samaras. Portrait lighting transfer using a mass transport approach. *ACM Transactions on Graphics (TOG)*, 37(1):2, 2018. 3
- [41] Z. Shu, E. Yumer, S. Hadap, K. Sunkavalli, E. Shechtman, and D. Samaras. Neural face editing with intrinsic image disentangling. In *Computer Vision and Pattern Recognition (CVPR), 2017 IEEE Conference on*, pages 5444–5453. IEEE, 2017. 2, 3
- [42] S. Suwajanakorn, I. Kemelmacher-Shlizerman, and S. Seitz. Total moving face reconstruction. In *ECCV*, 2014. 2
- [43] N. Wadhwa, R. Garg, D. E. Jacobs, B. E. Feldman, N. Kanazawa, R. Carroll, Y. Movshovitz-Attias, J. T. Barron, Y. Pritch, and M. Levoy. Synthetic depth-of-field with a single-camera mobile phone. *ACM Transactions on Graphics (TOG)*, 37(4):64, 2018. 8
- [44] Y. Wang, Z. Liu, G. Hua, Z. Wen, Z. Zhang, and D. Samaras. Face re-lighting from a single image under harsh lighting conditions. In *IEEE Conference on Computer Vision and Pattern Recognition*, pages 1–8, 2007. 2
- [45] Z. Wang, E. P. Simoncelli, and A. C. Bovik. Multiscale structural similarity for image quality assessment. In *The Thirtieth-Seventh Asilomar Conference on Signals, Systems & Computers, 2003*, volume 2, pages 1398–1402. Ieee, 2003. 6
- [46] Z. Wen, Z. Liu, and T. S. Huang. Face relighting with radiance environment maps. In *IEEE Conference on Computer Vision and Pattern Recognition*, 2003. 2
- [47] Y. Xiong, A. Chakrabarti, R. Basri, S. J. Gortler, D. W. Jacobs, and T. Zickler. From shading to local shape. In *PAMI*, 2014. 3, 4, 5
- [48] Z. Xu, K. Sunkavalli, S. Hadap, and R. Ramamoorthi. Deep image-based relighting from optimal sparse samples. *ACM Transactions on Graphics (TOG)*, 37(4):126, 2018. 2
- [49] E. Zhang, M. F. Cohen, and B. Curless. Emptying, refurbishing, and relighting indoor spaces. *ACM Transactions on Graphics*, 35(6), 2016. 2
- [50] E. Zhang, M. F. Cohen, and B. Curless. Discovering point lights with intensity distance fields. In *Proceedings of the IEEE Conference on Computer Vision and Pattern Recognition*, pages 6635–6643, 2018. 2
- [51] R. Zhang, P. Isola, A. A. Efros, E. Shechtman, and O. Wang. The unreasonable effectiveness of deep features as a perceptual metric. In *Proceedings of the IEEE Conference on Computer Vision and Pattern Recognition*, pages 586–595, 2018. 6, 8
- [52] R. Zhang, P.-S. Tsai, J. E. Cryer, and M. Shah. Shape-from-shading: a survey. *IEEE transactions on pattern analysis and machine intelligence*, 21(8):690–706, 1999. 2

## A. Supplementary Material

### A.1. Dataset Details

In order to balance the demographics of the captured data, we split the 21 subjects into a training, validation and test set according to Table 3, to achieve a meaningful distribution of salient characteristics in all of the subsets.

Table 3: **Dataset Details.** Considerations of salient characteristics to balance training, validation and test set.

	female	dark skin	glasses
training	2	3	4
validation	1	1	1
test	1	1	1
total	4	5	6
ratio	19.0%	23.8%	28.6%

### A.2. Dynamic Input Lighting

We illustrate the consistency and robustness of our approach by relighting multiple source light configurations to the same target lighting in Figs. 7 and 8. Our examples cover a wide spectrum of source illuminations, including strong and challenging directional lights originating on the side of the face. The extreme cases on the far left and right, in particular, require the removal of strong shadows. The noise in these low light areas is high, and visual cues are weak, which makes consistent relighting challenging.

### A.3. Extended Results

An extended comparison to related work can be found in Figs. 9 and 10. More results on relighting with an environment map are available in Figs. 11 and 12. Additional results of relighting under a moving target illumination can be found in the supplemental video<sup>5</sup>.

<sup>5</sup><https://youtu.be/QJK6MdT79rM>



Figure 7: **Dynamic Input Lighting.** In each row, we show a different facial expression that we relight from different input light configurations (columns; see small inset) to the same target light configuration. All results are based on our “full guidance” model and have been converted from linear to sRGB.



Figure 8: **Dynamic Input Lighting.** In each row, we show a different facial expression that we relight from different input light configurations (columns; see small inset) to the same target light configuration. All results are based on our “full guidance” model and have been converted from linear to sRGB.



Figure 9: **Extended Baseline Comparisons.** We compare relighting (a) the input image with (b/c) pretrained and retrained variants of SfSNet [37], (d) our model with no guidance as an extension of pix2pix [17], (e) our model with partial guidance on the normals, and (f) our model with full guidance. In (g), we show the ground truth capture of the given target illumination. All results have been converted from linear to sRGB.



Figure 10: **Extended Baseline Comparisons.** We compare relighting (a) the input image with (b/c) pretrained and retrained variants of SfsNet [37], (d) our model with no guidance as an extension of pix2pix [17], (e) our model with partial guidance on the normals, and (f) our model with full guidance. In (g), we show the ground truth capture of the given target illumination. All results have been converted from linear to sRGB.



Figure 11: **Relighting with Environment Maps.** We relight the input (first column) w.r.t. 5 different environment maps (small insets), ordered from cold (second column) to warm (sixth column) dominating color temperatures. All results have been converted from linear to sRGB.





Figure 12: **Relighting with Environment Maps.** We show the same type of visualization as in Fig. 11 but focus on more challenging scenarios, such as expressions affecting the face topology and glasses. All results have been converted from linear to sRGB.